OXFORD

Human Molecular Genetics, 2022, Vol. 31, 17, 2951–2963
https://doi.org/10.1093/hmg/ddac086
Advance access publication date: 13 April 2022
Original Article

An animal model for Pierpont syndrome: a mouse bearing the *Tbl1xr1* $^{Y446C/Y446C}$ mutation

Yalan Hu [1], Peter Lauffer[2], Michelle Stewart[3], Gemma Codner[3], Steffen Mayerl[4], Heike Heuer[4], Lily Ng[5], Douglas Forrest[5], Paul van Trotsenburg[2], Aldo Jongejan[6], Eric Fliers[7], Raoul Hennekam[8] and Anita Boelen[1,*]

[1]Endocrine Laboratory, Department of Clinical Chemistry, Amsterdam Gastroenterology, Endocrinology & Metabolism, Amsterdam UMC, University of Amsterdam, Amsterdam 1105AZ, The Netherlands
[2]Department of Pediatric Endocrinology, Emma Children's Hospital, Amsterdam Gastroenterology, Endocrinology & Metabolism, Amsterdam UMC, University of Amsterdam, Amsterdam 1105AZ, The Netherlands
[3]The Mary Lyon Centre, MRC Harwell, Harwell Campus, Oxfordshire OX11 0RD, UK
[4]Department of Endocrinology, Diabetes and Metabolism, University Hospital Essen, University of Duisburg-Essen, Essen 45122, Germany
[5]Laboratory of Endocrinology and Receptor Biology, National Institute of Diabetes and Digestive and Kidney Diseases, National Institutes of Health, Bethesda, MD 20892, USA
[6]Bioinformatics Laboratory, Department of Epidemiology and Data Science, Amsterdam Public Health, Methodology Amsterdam, Amsterdam UMC, University of Amsterdam, Amsterdam 1105AZ, The Netherlands
[7]Department of Endocrinology, Amsterdam Gastroenterology, Endocrinology & Metabolism, Amsterdam UMC, University of Amsterdam, Amsterdam 1105AZ, The Netherlands
[8]Department of Pediatrics, Emma Children's Hospital, Amsterdam UMC, University of Amsterdam, Amsterdam 1105AZ, The Netherlands
*To whom correspondence should be addressed at: Endocrine Laboratory, Amsterdam UMC, Academic Medical Center, Meibergdreef 9, 1105AZ Amsterdam, The Netherlands. Tel: +31 207325749; Email: a.boelen@amsterdamumc.nl

Abstract

Pierpont syndrome is a rare disorder characterized mainly by global developmental delay, unusual facial features, altered fat distribution in the limbs and hearing loss. A specific mutation (p.Tyr446Cys) in *TBL1XR1*, encoding a WD40 repeat-containing protein, which is a component of the SMRT/NCoR (silencing mediator retinoid and thyroid hormone receptors/nuclear receptor corepressors), has been reported as the genetic cause of Pierpont syndrome. Here, we used CRISPR-cas9 technology to generate a mutant mouse with the Y446C mutation in *Tbl1xr1*, which is also present in Pierpont syndrome. Several aspects of the phenotype were studied in the mutant mice: growth, body composition, hearing, motor behavior, thyroid hormone state and lipid and glucose metabolism. The mutant mice (*Tbl1xr1*$^{Y446C/Y446C}$) displayed delayed growth, altered body composition with increased relative lean mass and impaired hearing. Expression of several genes involved in fatty acid metabolism differed in white adipose tissue, but not in liver or muscle of mutant mice compared to wild-type mice (*Tbl1xr1*$^{+/+}$). No difference in thyroid hormone plasma concentrations was observed. *Tbl1xr1*$^{Y446C/Y446C}$ mice can be used as a model for distinct features of Pierpont syndrome, which will enable future studies on the pathogenic mechanisms underlying the various phenotypic characteristics.

Introduction

Pierpont syndrome is a rare disorder with autosomal dominant inheritance that manifests with global development delay, variable degrees of intellectual disability, distinct facial characteristics, impaired hearing, motor defects and altered fat distribution in the distal limbs (1–4). It was first reported in 1998 by Dr Mary Ella Mascia Pierpont *et al.* in two boys with global developmental delay, facial abnormalities, microcephaly, bilateral congenital fat pads anteromedial to the heels and palmar and plantar fat accumulations (1). In 2005, Oudesluijs *et al.* (2) reported another boy with a similar phenotype and suggested to call this combination of symptoms Pierpont syndrome. In Pierpont's initial report, there was no description of hearing loss in the initial patient, and the hearing of the second patient was initially described as normal. However, after a follow-up period of 6 years the second patient showed unilateral hearing loss (2). In a more recent paper, all five reported patients had (audiometry proven) hearing loss (4).

We identified a single heterozygous missense variant, c.1337A>G (p.Tyr446Cys), in transducin β-like 1 X-linked receptor 1 (*TBL1XR1*) in six patients with Pierpont syndrome (4). *TBL1XR1* is a member of the WD40 repeat-containing gene family. The WD40 domain consists of 4–8 WD40 repeat and folds into a β-propeller structure, providing a platform for the interaction and assembly of several proteins into a signalosome. The WD40 domain interacts with proteins and DNA and is involved in a wide range of cellular functions (5). In general, WD40 domain proteins coordinate ubiquitination, histone methylation (6) and acetylation (4).

TBL1X, short for transducin beta like 1 X-linked, is another member of the WD40 repeat-containing gene

Received: January 17, 2022. **Revised:** March 23, 2022. **Accepted:** April 7, 2022

family and shares high sequence similarity with *TBL1XR1* (86%). Notably, a mutation in *TBL1X* at an identical position in the WD40 domain as observed in *TBL1XR1* results in a different phenotype in patients, i.e. isolated central congenital hypothyroidism [CH-C (4)]. The term central CH refers to a congenital shortage of thyroid hormone as a result of insufficient thyroid-stimulating hormone (TSH) production and/or release at the level of the pituitary and/or impaired stimulation of the pituitary by thyrotropin-releasing hormone (TRH) in the hypothalamus. Thyroid hormone is indispensable for growth, development and auditory function (7). Interestingly, patients with a mutation in *TBL1X* showed also impaired hearing (8), a symptom observed in patients with Pierpont syndrome too. Moreover, a mutation in *TBL1Y*, a homolog at chromosome Y, has been reported to be associated with hearing loss as well (9).

TBL1XR1 is expressed in various brain areas including the hypothalamus and pituitary, white and brown adipose tissue (WAT and BAT), muscle and liver (4). At present, it is unknown which genes and molecular mechanisms are involved in the pathogenesis of the Pierpont phenotype. In the present study, we developed a mouse model bearing the *Tbl1xr1* Y446C mutation in both alleles in order to study its effects on growth, hearing, psychomotor development and a variety of target tissues including WAT, BAT, liver and muscle. To this end, we measured body composition, the auditory evoked brainstem response (ABR) and gene expression of a variety of genes involved in lipid metabolism in liver, muscle and adipose tissue, both in mice carrying the mutation and wild-type (WT) mice. Psychomotor development was assessed by measuring locomotor coordination. As the identical mutation in *TBL1X* resulted in central-CH (CH-C), we also studied plasma thyroid hormone concentrations as well as hypothalamic *Trh* mRNA expression in these mice.

Results

Generation of the *Tbl1xr1* $^{Y446C/Y446C}$ mice

Using CRISPR-Cas9 technology, we generated a homozygous mouse model of Pierpont Syndrome containing a Y446C point mutation in exon 14 of *Tbl1xr1* resulting in an amino acid change from tyrosine to cysteine (Fig. 1A). The mutation is located in the WD40 domain of the protein. The F0 generation was mated with WT C57BL/6J mice of the same age to obtain a F1 generation. Subsequently, mature F1 mice were backcrossed to obtain a F2 generation *Tbl1xr1*$^{Y446C/+}$ mouse and the F2 generation was intercrossed to obtain homozygous *Tbl1xr1*$^{Y446C/Y446C}$ mice (Fig. 1B).

Body composition

To evaluate the effect of the *Tbl1xr1* mutation on growth, body weight was recorded weekly between postnatal week 4 and 10. Body weight of male *Tbl1xr1*$^{Y446C/Y446C}$ mice was lower as compared to male *Tbl1xr1*$^{+/+}$ mice at all time points (Fig. 2A). No differences were observed between female *Tbl1xr1*$^{Y446C/Y446C}$ and *Tbl1xr1*$^{+/+}$ mice.

Tbl1xr1$^{Y446C/Y446C}$ mice displayed higher lean mass and lower fat mass compared to *Tbl1xr1*$^{+/+}$ mice (Fig. 2B and C). No sex difference was observed in percentage lean and fat mass (data not shown).

Bone

To evaluate the effect of the mutation on bone, we measured bone mineral density (BMD) and bone mineral composition (BMC). BMD was lower in both male and female *Tbl1xr1*$^{Y446C/Y446C}$ mice compared to *Tbl1xr1*$^{+/+}$ mice (Fig. 3A). BMC was lower only in male *Tbl1xr1*$^{Y446C/Y446C}$ mice (Fig. 3B).

Hearing

Hearing was assessed by testing the ABR, an overall indicator of auditory function. The ABR thresholds were moderately elevated in *Tbl1xr1*$^{Y446C/Y446C}$ mice compared to *Tbl1xr1*$^{+/+}$ mice in response to a range of stimuli (8, 16, 32 kHz and a click stimulus), as measured in combined groups of males and females (Fig. 4A). Histological analysis of the cochlea of adult mice did not reveal obvious morphological abnormalities. Figure 4B shows representative sections in the region of the organ of Corti with no overt defects observed in mutant mice compared to control mice.

Locomotor activity

Mice underwent the Locotronic® test, which was used to evaluate motor coordination and activity. No differences were observed in locomotor activity between *Tbl1xr1*$^{Y446C/Y446C}$ and *Tbl1xr1*$^{+/+}$ mice (Fig. 5).

Hypothalamus–pituitary–thyroid axis

No differences in serum T4, T3, and TSH concentrations or hypothalamic *Trh* mRNA were observed between *Tbl1xr1*$^{Y446C/Y446C}$ and *Tbl1xr1*$^{+/+}$ mice. We did find gender differences with lower serum T3 and TSH and higher absolute hypothalamic *Trh* mRNA in female mice (Fig. 6). However, the gender-related differences were similar in *Tbl1xr1*$^{Y446C/Y446C}$ and *Tbl1xr1*$^{+/+}$ mice.

Genes involved in fat metabolism in BAT, WAT, liver and muscle

The mutated *Tbl1xr1* did not affect genes involved in lipid metabolism in BAT, liver or gastrocnemius muscle. Three genes displayed a gender difference; *Ucp1* in BAT, *Ppara* and *Fasn* in liver. The gender differences did not differ between *Tbl1xr1*$^{Y446C/Y446C}$ and WT mice. However, increased expression of three genes (*Ppara*, *Ucp1* and *Fasn*) in WAT was observed in the *Tbl1xr1*$^{Y446C/Y446C}$ mice compared to WT mice (Fig. 7). No difference was observed in the expression of genes involved in glucose metabolism in any of the four organs (Supplementary Material). To further explore the differentially expressed genes in WAT of WT and *Tbl1xr1*$^{Y446C/Y446C}$ mice, RNA-seq was performed in WAT. Gene Set Enrichment Analysis

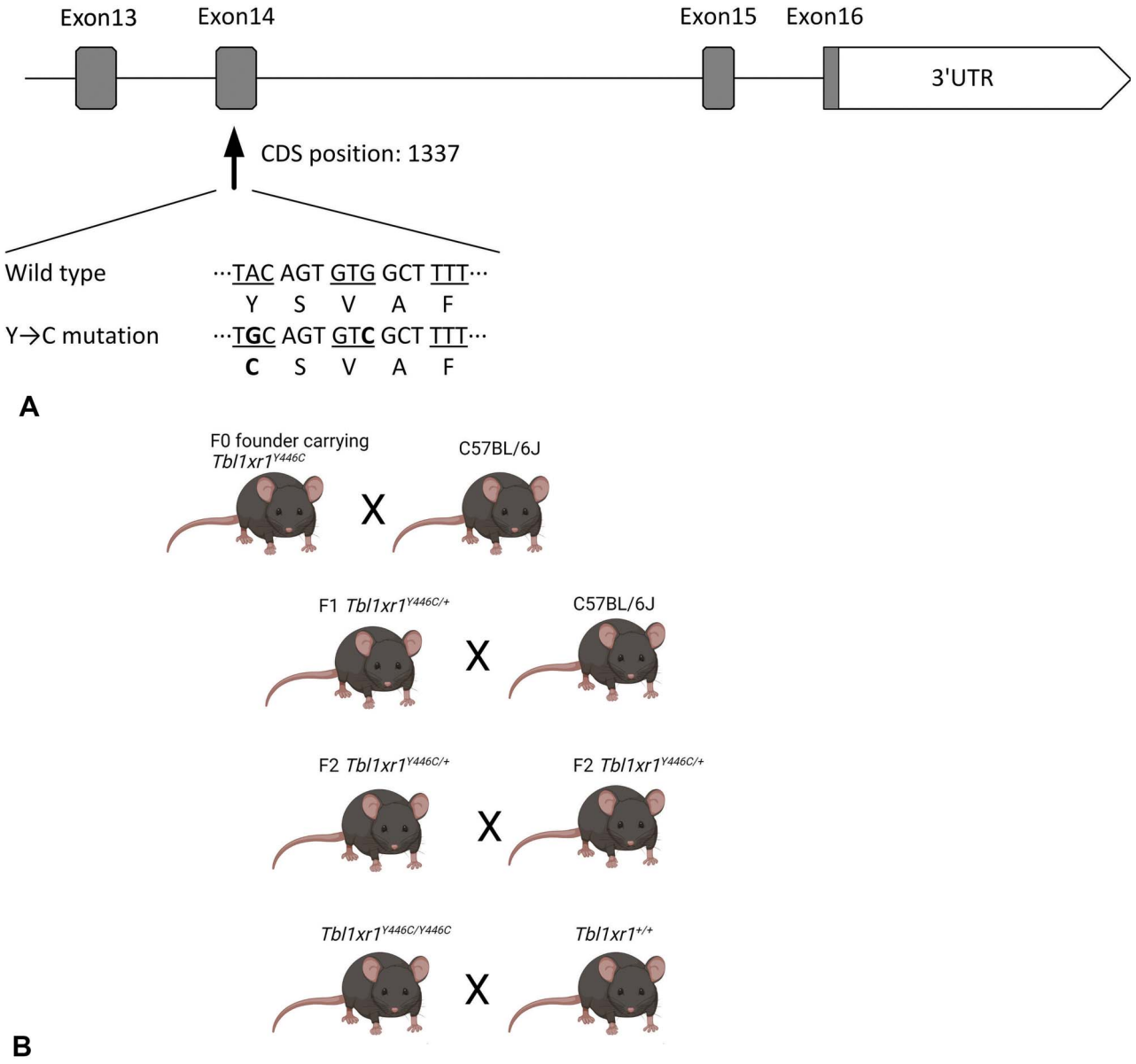

Figure 1. Generation of the *Tbl1xr1*$^{Y446C/Y446C}$ mouse line. (**A**) Representative view of the CRISPR/Cas9 targeting strategy used for generating *Tbl1xr1*$^{Y446C/Y446C}$ mice. Using CRISPR/Cas9, a tyrosine-to-cysteine missense mutation (Y446C) was generated in exon 14 of the mouse sequences of the mouse *Tbl1xr1* locus. A silent mutation (G>C) was generated to remove the PAM site without changing the protein sequence. The nucleotide and amino acid of WT and mutant alleles (in bold) are shown. Exons are indicated with gray boxes and introns are noted by gray lines. The targeting site is indicated by a black arrow. (**B**) Breeding strategy to obtain *Tbl1xr1*$^{Y446C/Y446C}$ mice. Founder mice were crossed to C57BL/6J to generate F1s, then F1s crossed to C57BL/6J to generate F2s. F2s were intercrossed for generating the respective cohorts.

(GSEA) revealed 11 gene sets (using the search terms 'ADIPOGENESIS' and 'ADIPOGENIC') related to adipogenesis that showed significant changes in expression [false discovery rate (FDR) < 0.05] between WT and *Tbl1xr1*$^{Y446C/Y446C}$ mice (see Table 2). We excluded one of these as it focused on adipogenesis in BAT (M8364). All remaining 10 gene sets were established in 3T3-L1 cells that were differentiated into adipocytes using a variety of inducers [such as thiazolidinediones (TZDs) and IDX (insulin, dexamethasone, isobutylmethylxanthine)]. The direction of differential expression of four of the ten gene sets (M1579, M1577, M1626 and M2271—containing genes related to either positive or negative regulation of adipogenesis) was indicative of increased adipogenesis in WAT of *Tbl1xr1*$^{Y446C/Y446C}$ mice (Table 2). However, the remaining gene sets (M2432, M2270, M1645, M2420, M1675 and M2182—all containing genes related to positive regulation of adipogenesis) were downregulated in WAT of *Tbl1xr1*$^{Y446C/Y446C}$ mice, indicating reduced adipogenesis.

Discussion

In this study, we used CRISPR-Cas9 technology to generate mice bearing the Y446C mutation in *Tbl1xr1* to establish an animal model for Pierpont syndrome. We

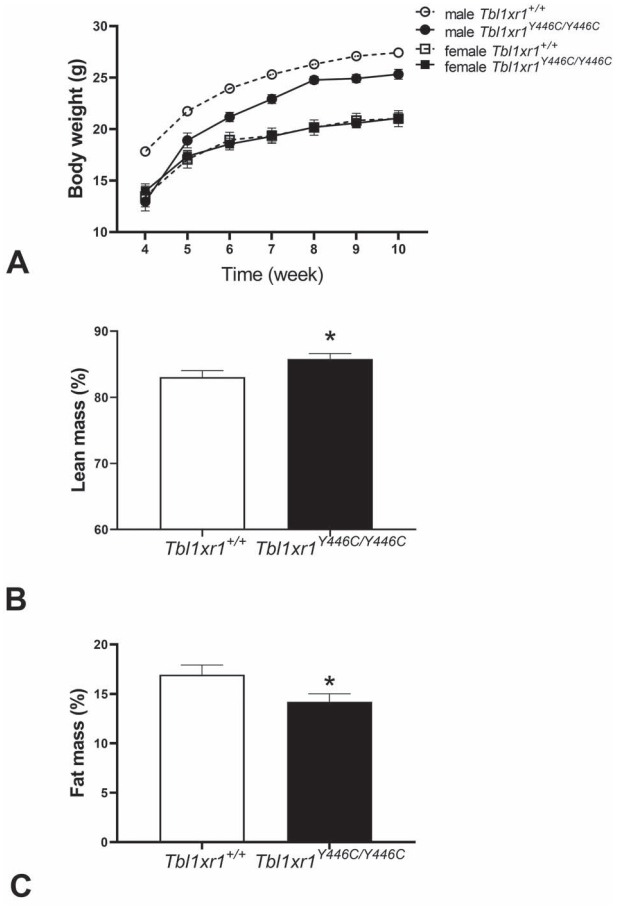

Figure 2. Body weight (**A**), percentage of lean mass (**B**) and fat mass (**C**) in *Tbl1xr1*$^{Y446C/Y446C}$ mice compared to age- and sex-matched *Tbl1xr1*$^{+/+}$ mice. White bars indicate *Tbl1xr1*$^{+/+}$ and black bars indicate *Tbl1xr1*$^{Y446C/Y446C}$ mice. Data are expressed as mean ± SEM; 6–7 animals per group (A) and 12–14 animals per group including both males and females since there is no gender difference (B, C). Differences between groups were analyzed using two-way ANOVA; *($P < 0.05$).

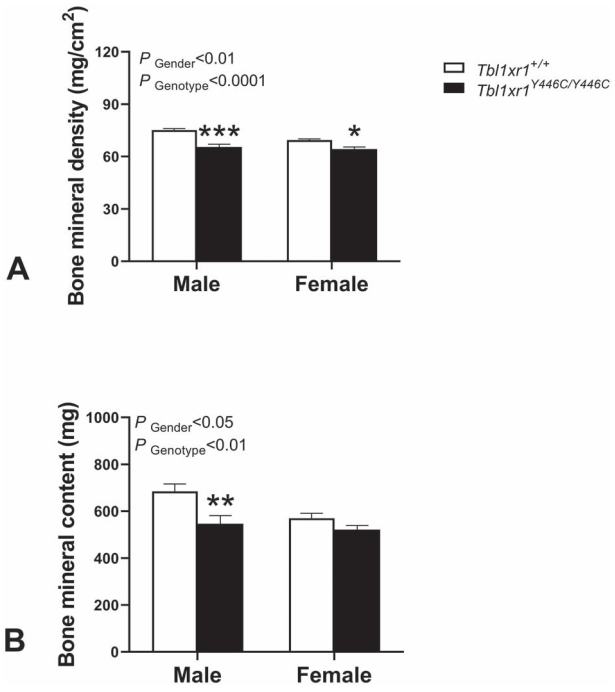

Figure 3. BMD (**A**) and BMC (**B**) in *Tbl1xr1*$^{Y446C/Y446C}$ mice compared to age- and sex-matched *Tbl1xr1*$^{+/+}$ animals. White bars indicate *Tbl1xr1*$^{+/+}$ and black bars indicate *Tbl1xr1*$^{Y446C/Y446C}$ mice. Data are expressed as mean ± SEM; 6–7 animals per group; differences between groups were analyzed using two-way ANOVA; *($P < 0.05$), **($P < 0.01$), ***($P < 0.001$).

evaluated various aspects of the human phenotype (growth, motor development, hearing and WAT) in these mice in order to study the functional consequences of the mutation at the tissue level. As an identical mutation in the highly homologous gene *TBL1X* results in CH-C, we also studied thyroid function in the mice. The main finding of the study is that the homozygous Y446C mutation in mice recapitulates several of the main features of Pierpont syndrome, i.e. growth retardation, hearing loss and altered body composition. This may guide future studies on the molecular mechanisms underlying Pierpont syndrome and the main phenotype characteristics.

Our study is the first describing the phenotype of mice bearing a mutation in Tbl1xr1 and linking this to Pierpont syndrome. However, studies have been described wherein TBL1RX1 is either overexpressed or deficient. Overexpression of TBL1R1 is associated with a worse prognosis of gastric cancer (10) while deficiency of Tbl1xr1 causes asthenozoospermia (11).

A major difference between humans and mice is that the heterozygous mouse does not show a detectable phenotype while in humans the heterozygote shows Pierpont syndrome, and only the homozygous mice mimic the heterozygous human phenotype. It is not uncommon that variants in genes act differently in mice and humans and that mutated genes that cause a phenotype in humans do not cause a phenotype in mice. The background varies, several mechanisms exist, often as a result of evolutionary adaptations in humans, paralogous gene duplication events in mice and similar mechanisms. For instance, homologous genes may exist in different copies, evident also in man for *TBL1XR1*, as at least two other genes (*TBL1X* and *TBL1Y*) exist with a high sequence similarity and to some extent a similar function (evident through the hearing loss that occurs in variants of each of these genes). Mechanisms are even more complex as many proteins act in protein complexes and also ligand–receptor interactions are involved, so phenotypes are caused by a combination of proteins. A well-known phenomenon is a dominant-negative effect (in the heterozygote binding of the mutated protein to the normal protein causes inactivation of the complete complex, so of normal protein as well) that may be present in the human and not in the mouse. At present, we do not know what the explanation is for the difference in the functioning of Tbl1xr1 in mice and TBL1XR1 in humans.

Growth and body composition

We observed that the weight gain of male *Tbl1xr1*$^{Y446C/Y446C}$ mice lagged significantly behind that of male *Tbl1xr1*$^{+/+}$ mice, but there was no difference in body weight of

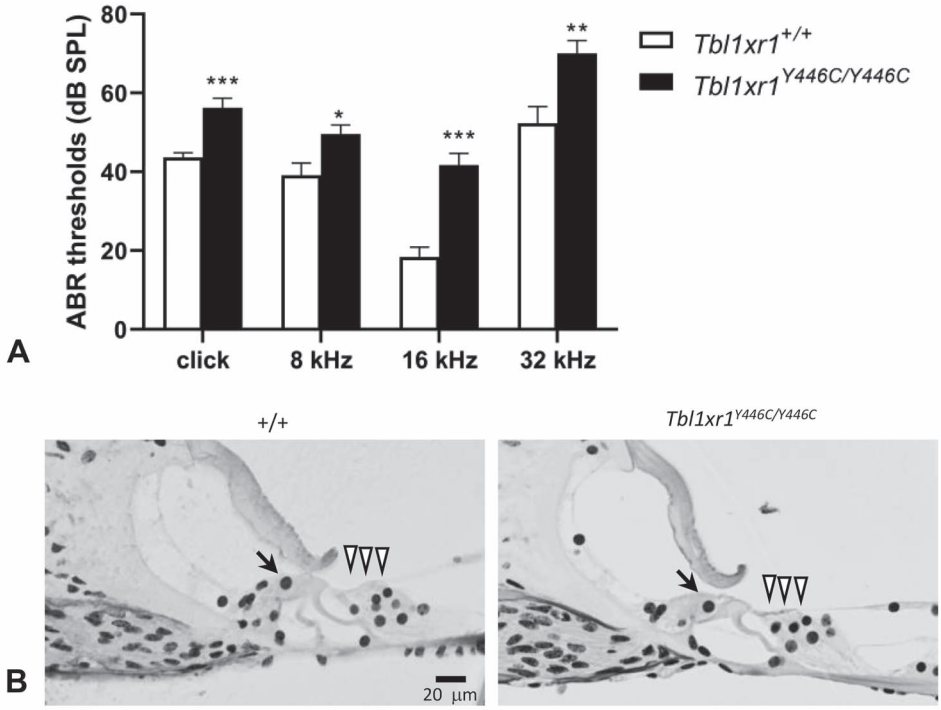

Figure 4. (**A**) ABR in *Tbl1xr1*$^{Y446C/Y446C}$ mice compared to age-matched *Tbl1xr1*$^{+/+}$ animals. Average thresholds are shown for different stimuli (click, 8, 16, 32 kHz) for mice at 3–5 months of age; $n = 11$ per group including both males and females since there is no gender difference. White bars indicate *Tbl1xr1*$^{+/+}$ and black bars indicate *Tbl1xr1*$^{Y446C/Y446C}$ mice. Data are expressed as mean ± SEM; difference between *Tbl1xr1*$^{+/+}$ and *Tbl1xr1*$^{Y446C/Y446C}$ groups was analyzed using two-way ANOVA for each stimulus; *($P < 0.05$), **($P < 0.01$), ***($P < 0.001$). (**B**) Histology of the cochlea. Six μm plastic sections of a representative mid-basal turn of the cochlea showing a lack of obvious abnormalities in inner hair cells (arrow) or outer hair cells (arrowheads) or the organ of Corti in *Tbl1xr1*$^{Y446C/Y446C}$ mice.

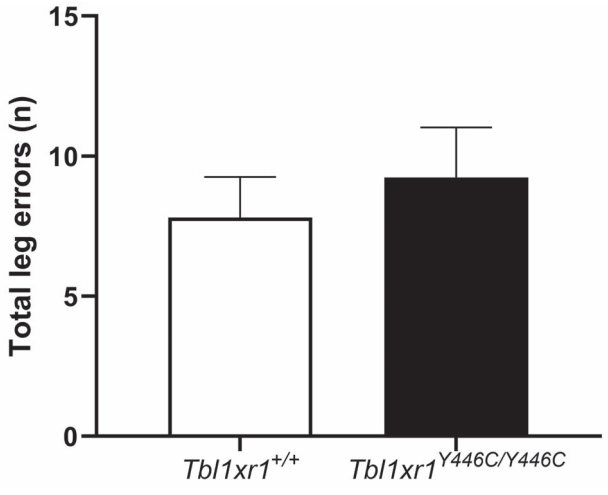

Figure 5. Total leg errors (front leg and rear leg) as a read out for locomotor activity in *Tbl1xr1*$^{Y446C/Y446C}$ mice compared to age- and sex-matched *Tbl1xr1*$^{+/+}$ animals in week 10. Data are expressed as mean ± SEM; 6–7 animals per group; differences between groups were analyzed using two-way ANOVA. Since there is no gender difference, combined data of male and female are shown.

female *Tbl1xr1*$^{Y446C/Y446C}$ and *Tbl1xr1*$^{+/+}$ mice. In humans with Pierpont syndrome, both male and female patients display growth retardation, i.e. decrease in height and weight compared to age-matched controls. Thus, the mouse phenotype is only partly mimicking the human phenotype in this respect.

We observed an increased percentage of lean mass and a decreased percentage of fat mass in the *Tbl1xr1*$^{Y446C/Y446C}$ mice, indicating that the *Tbl1xr1*$^{Y446C/Y446C}$ mice had a leaner phenotype. It remains unknown at present whether the leaner phenotype of the *Tbl1xr1*$^{Y446C/Y446C}$ mice is present in humans with Pierpont syndrome since such data are not available. We do know that fat distribution in Pierpont syndrome patients is abnormal in the distal limbs, that both height and weight are below the 50th centile in all patients reported to date except one and that in half of the reported patients body weight is at a clearly lower centile than height; this may be an indication of an altered body composition in humans as well.

Bone

BMC and BMD of *Tbl1xr1*$^{Y446C/Y446C}$ mice were lower than those of *Tbl1xr1*$^{+/+}$ mice. Bone density data have not been reported in humans with Pierpont syndrome. It is, therefore, of interest to measure bone parameters in patients with Piermont syndrome in the future.

Hearing

The higher hearing threshold in *Tbl1xr1*$^{Y446C/Y446C}$ mice compared to *Tbl1xr1*$^{+/+}$ mice reflects moderate hearing loss. This is consistent with the impaired hearing reported in most patients with Pierpont syndrome (4,12). The mouse model may be of value to explore the

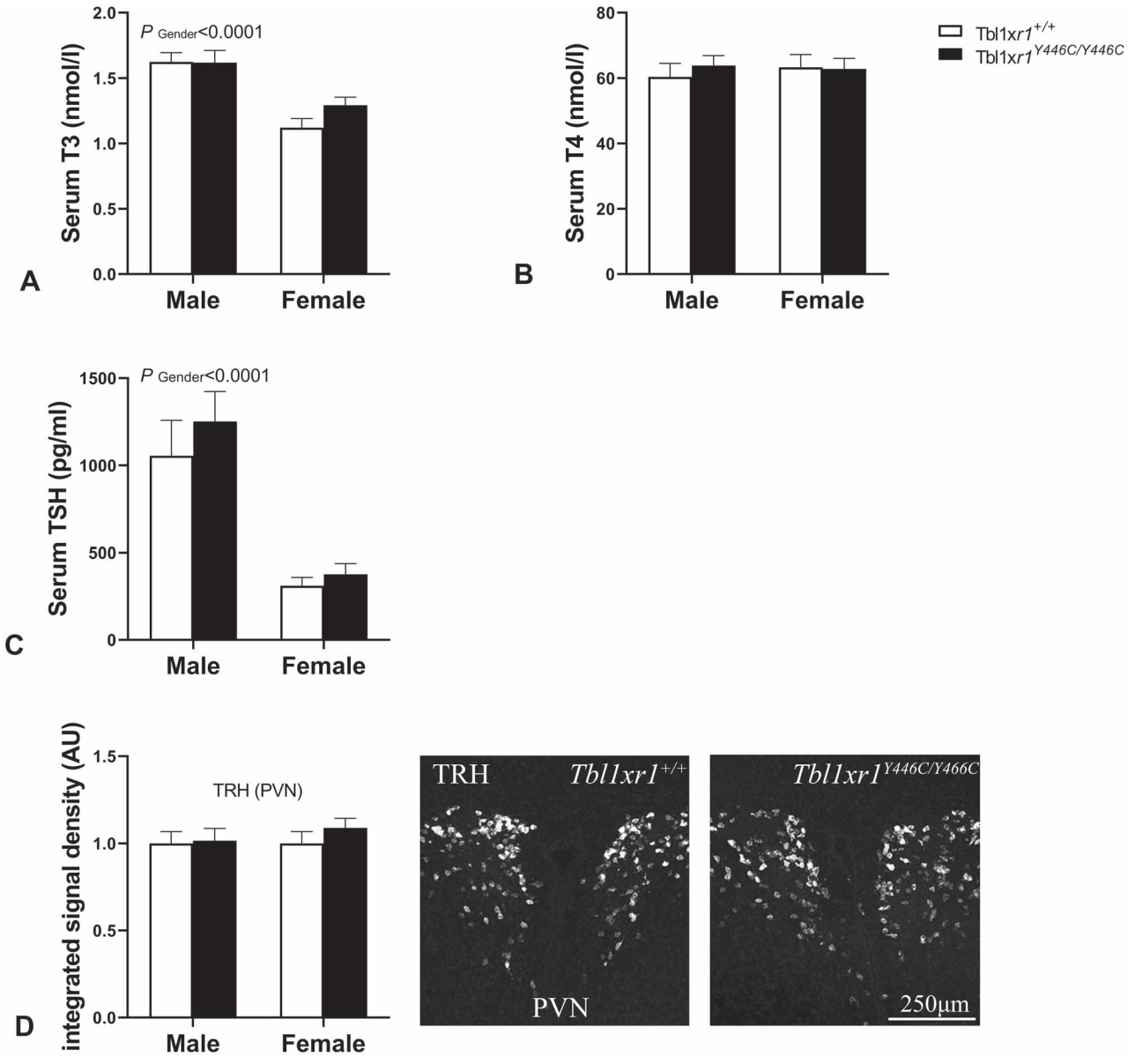

Figure 6. Characterization of the hypothalamus–pituitary–thyroid axis in *Tbl1xr1*$^{Y446C/Y446C}$ mice compared to age- and sex-matched *Tbl1xr1*$^{+/+}$ animals. (**A**) Serum T4 concentrations, (**B**) serum T3 concentrations, (**C**) serum TSH concentrations, (**D**) normalized TRH expression in the hypothalamic PVN in both male and female mice (female and male WT animals are set as 1). White bars indicate *Tbl1xr1*$^{+/+}$ and black bars indicate *Tbl1xr1*$^{Y446C/Y446C}$ mice. Data are expressed as mean ± SEM; 6–7 animals per group; differences between groups were analyzed using two-way ANOVA. The photograph shows representative TRH mRNA expression using FISH in the PVN of female *Tbl1xr1*$^{+/+}$ and *Tbl1xr1*$^{Y446C/Y446C}$ mice.

mechanism behind impaired hearing in the patients. In addition, mutations in two other genes homologous to *TBL1XR1*, i.e. *TBL1X* and *TBL1Y*, have also been found to be associated with hearing impairment (8,9,13). Perhaps, TBL1XR, TBL1X and TBL1Y play an overlapping but independent role in the process of auditory development. If these related factors can compensate for each other *in vivo*, this may in part account for the variable observation of hearing loss in Pierpont syndrome. The hearing loss is unlikely to be associated with the mild hypothyroidism observed in patients with mutations in *TBL1X*, as mutations in *TBL1XR1* and *TBL1Y* are unrelated to central hypothyroidism and the mouse models do not have altered thyroid hormone concentrations. The underlying defects may be subtle as histological analysis showed no obvious morphological abnormalities of the cochlea, presumably consistent with the moderate degree of hearing loss.

Locomotor activity

We did not observe impaired locomotor behavior in the *Tbl1xr1*$^{Y446C/Y446C}$ mice. This contrasts with patients who show significant motor retardation as part of their global development delay (1–4). Still, the number of locomotor errors in the mutant mouse group was slightly higher than that in the WT group but the difference was not statistically significant. In future studies, additional and perhaps more sensitive locomotor tests including

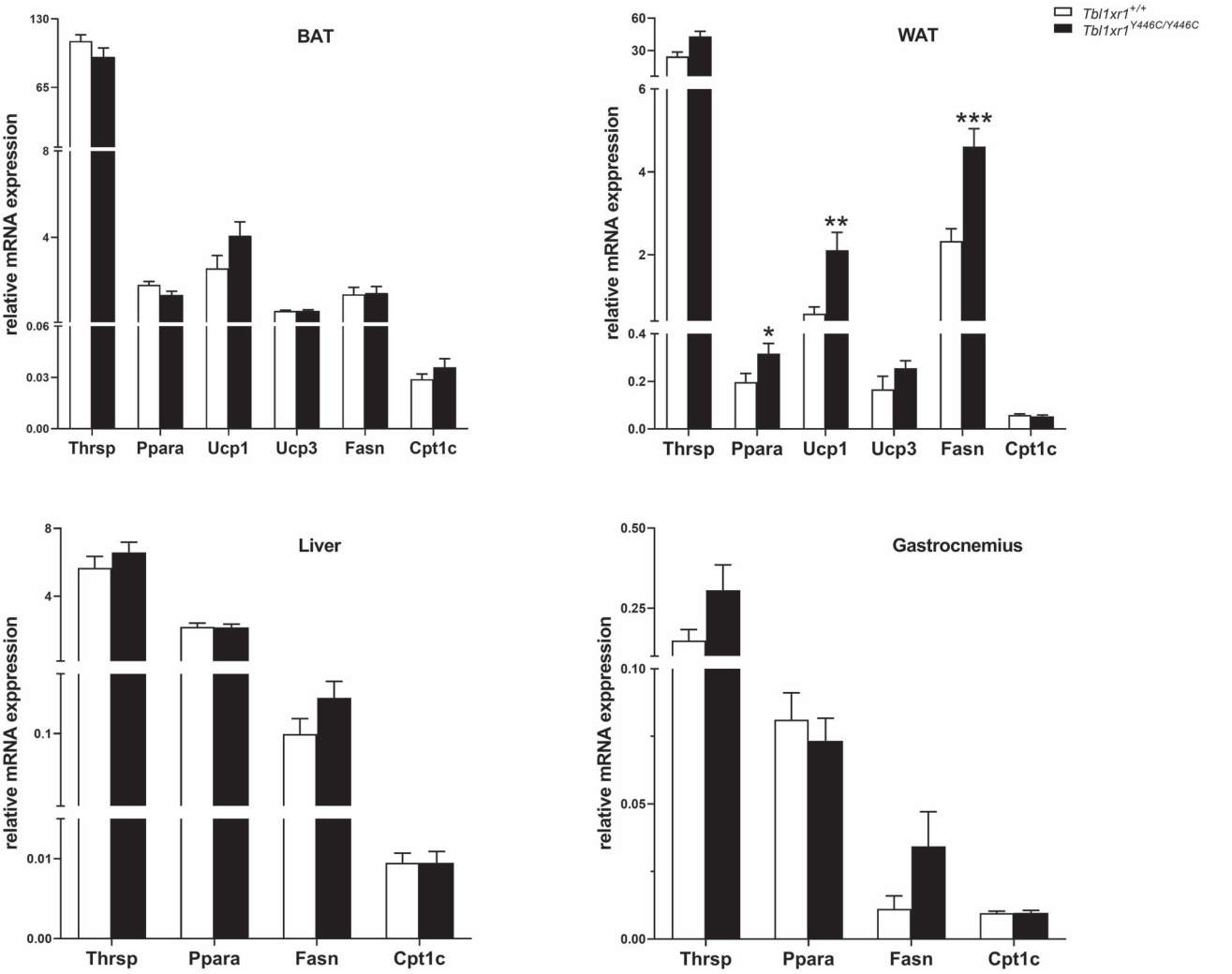

Figure 7. Relative mRNA expression of genes involved in fatty acid metabolism in peripheral tissues (BAT, WAT, liver and gastrocnemius muscle) in *Tbl1xr1*$^{Y446C/Y446C}$ mice compared to age- and sex-matched *Tbl1xr1*$^{+/+}$ mice. Measurements by qPCR analysis. Since there is no gender difference in most of the genes except *Ucp1* in BAT and *Pparα* and *Fasn* in liver, combined data of male and female are shown. White bars indicate *Tbl1xr1*$^{+/+}$ and black bars indicate *Tbl1xr1*$^{Y446C/Y446C}$ mice. Data are expressed as mean ± SEM; 6–7 animals per group; differences between groups were analyzed using two-way ANOVA; *($P < 0.05$), **($P < 0.01$), ***($P < 0.001$).

the balance beam test and hanging tail test should be used to investigate this aspect in more detail and to detect more subtle locomotor deficits in this mouse model.

Genes involved in fat metabolism in WAT, liver and muscle

To explore whether the mutation affects glucose and fatty acid metabolism in key metabolic organs, we analyzed several genes involved in glucose and fatty acid metabolism in liver, muscle, BAT and WAT. The mutation had no detectable effect on glucose and lipid metabolism in most tissues. However, three key genes in fatty acid metabolism (*Ppara*, *Ucp1*, *Fasn*) showed increased mRNA expression in WAT.

Peroxisome proliferator-activated receptors (PPARs) are transcription factors that belong to the superfamily of nuclear receptors. Activation of PPAR*α* reduces triglyceride level and increases FA uptake and oxidation (14). UCP1 is a protein mediating cold-, sympathetic nervous system- and thyroid hormone-stimulated BAT thermogenesis (15–17). Activation of PPAR*α* by lipolysis-derived fatty acids contributes to the coordination of *Ucp1* gene transcription (thermogenesis) (18).

The increased expression of *Ppara* (18–21) and *Ucp1* mRNA suggests that WAT has a tendency of browning (22,23), which may be partly responsible for the reduced weight gain of *Tbl1xr1*$^{Y446C/Y446C}$ mice and the leaner phenotype of *Tbl1xr1*$^{Y446C/Y446C}$ mice since browning was found to be beneficial in terms of reduction of body weight and improvement of insulin sensitivity (24).

Fatty acid synthase (FASN), encoded by *Fasn*, is the key enzyme for *de novo* lipogenesis (24,25). Cellular FASN expression is physiologically upregulated in a state of energy excess (25) and increased FASN gene expression in adipose tissue is linked to visceral fat accumulation and impaired insulin sensitivity (26), which is contradictory to the effect of browning. Increased FASN expression, however, fits with the phenotype of the patients as they have fat pads in the limbs suggesting fat accumulation.

Fat pads in hands and feet, observed in Pierpont patients but not in the mutant mice, are compatible with an enhanced local adipogenesis while a leaner phenotype may indicate a reduced adipogenesis. However, a lean phenotype might also be due to other mechanisms, especially an enhanced metabolism, which we were not able to study in the mice. RNA-seq analysis revealed gene sets that were downregulated in *Tbl1xr1*$^{Y446C/Y446C}$ mice fitting with less adipogenesis but also gene sets with changes suggesting increased adipogenesis. Adipose development is an extremely complex developmental process, which is regulated by a large number of factors (27). Environmental factors such as temperature or diet affect adipocyte gene expression by epigenetic events (28). In Pierpont syndrome, fat pads are solely located at hands and feet. This suggests local dysregulation of adipogenesis possibly involving local external factors. We hypothesize that variants in *TBL1R1* that result in Pierpont syndrome alone are not sufficient to result in a locally disturbed adipogenesis and that additional, yet unknown, external factors are essential for the development of fat pads.

Of note, the increased expression of both *Fasn* mRNA and *Ucp1* mRNA was also observed in the mouse model of chronic β3-adrenergic receptor activation (29), which shows more browning and a leaner phenotype, similar to our mouse model. However, the link between *Tbl1xr1* and adrenergic stimulation is unknown at present.

In summary, we have generated a mouse model for Pierpont syndrome using the CRISPR-Cas 9 technology, which successfully mimics several but not all aspects of the human phenotype. The current mouse model can be of value for future studies on the pathogenesis of the syndrome and several of its main characteristics, especially the altered body composition and hearing loss.

Materials and Methods

The generation of targeted mice bearing the *Tbl1xr1* $^{Y446C/Y446C}$ mutation

Targeted mice bearing the *Tbl1xr1*$^{Y446C/Y446C}$ mutation, named TBL1XR1-Y446C-EM1-B6, were generated at MRC Harwell (Didcot, UK) using CRISPR-Cas9 technique. A sgRNA (sequence 5′-TCAAGAGCCCGTGTACAGTGTGG-3′) targeting *Tbl1xr1* exon 14 was synthesized *in vitro* (Fig. 1). Cas9 mRNA, sgRNAs and donor DNA (sequence ssODNs 5′-GCCAGATACCTGCCATCAGGACTAAAAGCGACACTGCA CACGGGCTCTTGATGTTTTGTCAAAGTATGGATGCAAATC CCTCTGTCTACGTCCCATAACCTA-3′) were microinjected into fertilized one-cell embryos of C57BL/6J mice. The injected one-cell embryos were transferred into the pseudopregnant female mice. The presence of genomic modification in the F0 generation was determined by genomic DNA analysis via PCR and Sanger sequencing on ear clip samples [see Supplementary Material as described in (30)]. F0 generation mice were mated with WT C57BL/6J mice of the same age to obtain F1 generation mice. These mice underwent PCR and Sanger sequencing to enable definite characterization of the mutant allele. Animals that showed the desired base changes also underwent copy counting analysis via digital droplet PCR to check against additional donor integrations in the genome. Subsequently, mature F1 generation mice were backcrossed to obtain F2 generation *Tbl1xr1*$^{Y446C/+}$ mice and F2 generation were intercrossed to obtain homozygous *Tbl1xr1*$^{Y446C/Y446C}$ mice. All F2 offsprings were genotyped by qPCR.

All procedures conducted were done so in accordance with the Animals (Scientific Procedures) Act 1986 Amendment Regulations 2012 (SI 4 2012/3039) at Harwell (Didcot, UK). Mice were housed in Tecniplast IVC cages (1284L and 1285L) with Aspen bedding (Datesand). Food and water were provided *ad libitum*. The lighting regime was 12 h light, 12 h dark with 30 min dusk to dawn, dawn to dusk period. Health checks were conducted daily and a maximum number of five animals were housed per cage. Male and female mice were used at the age of 10–12 weeks. For auditory testing, mice were maintained and analyzed at NIDDK, National Institutes of Health under approved protocols and following the guidelines for care at the National Institutes of Health.

Genotyping

F0 and F1 samples were genotyped by qPCR and sequencing. F2 offspring and subsequence generations were genotyped by qPCR. Mouse ear DNA was extracted using the DNA Extract All Reagents Kit (Thermo Fisher Scientific) and stored at −20°C until use. Samples were genotyped using qPCR with a FAM-labeled TaqMan assay (LGC, Biosearch Technologies, 5 μM probe, 15 μM each primer) designed to detect either the WT *Tbl1xr1* allele or the mutant *Tbl1xr1* allele, run in multiplex with a VIC-labeled internal control *Dot1L* (Thermo Fisher Scientific, 5 μM probe, 20 μM each primer), TaqMan GTXpress Master Mix (Thermo Fisher Scientific) and 1:10 dilution of DNA Extract All Reagents Kit preparation.

Body weight and body composition

Body weight was weekly recorded from week 4 to week 10. Body composition and BMD and BMC of anesthetized mice at the age of 11 weeks were assessed using the PIX-Imus Dual Energy X-Ray Absorption machine (GE Medical Systems, USA), the so-called DEXA system. The PIX-IMUS Densitometer provides BMD and body composition results from total body imaging in less than 5 min by taking high-energy X-ray images. Results include BMD in mg/cm^2, BMC in mg, bone area in cm^2, % fat, lean tissue in grams, and fat tissue in grams.

Hearing and histology of the cochlea

Auditory function was measured in male and female mice using a Smart EP system (Intelligent Hearing System, Miami, FL) to test the ABR under avertin anesthesia (0.25 mg/g body weight), as described in (31). Two independent groups of mice at 3–5 months of age were tested. No differences in outcomes were observed

Table 1. List of primers used for qPCR

Gene name	Symbol	Primer	Forward (5′–3′)	Reverse (5′–3′)	Products length (bp)
Eukaryotic translation elongation factor 1 alpha 1	Eef1a1	mmEF1a1a	AGTCGCCTTGGACGTTCTT	ATTTGTAGATCAGGTG-GCCG	174
Ribosomal protein, large, P0	Rplp0	RPLP-1	GGCCCTGCACTCTCGCTTTC	TGCCAGGACGCGCTTGT	124
Hypoxanthine guanine phosphoribosyl transferase	Hprt	mmHPRT	GCAGTACAGCCCCAAAATGG	AACAAAGTCTGGCCTG-TATCCAA	84
Solute carrier family 2 (facilitated glucose transporter), member 4	Slc2a4	mmGLUT4	TCCCTTCAGTTTGGCTATAA-CATTG	ACGTTGCATTGTAGCTCT-GTTCA	69
Malic enzyme 1, NADP(+)-dependent, cytosolic	Me1	mmME	GAAAGAGGTGTTTGCC-CATGA	AATTGCAGCAACTCCTAT-GAGG	96
Phosphoenolpyruvate carboxykinase 1, cytosolic	Pck1	mmPEPCK	ATGTTCGGGCGGATTGAAG	TCAGGTTCAAG-GCGTTTTCC	81
Peroxisome proliferative activated receptor Gamma, Coactivator 1 alpha	Ppargc1a	mmPGC1a	CAATGAATGCAGCGGTCTTA	GTGTGAGGAGGGT-CATCGTT	197
Thyroid hormone responsive	Thrsp	mmSpot14	CATCCTTACCCACCTGACCC	TGTCCAGGTCTCGGGTTGAT	157
Peroxisome Proliferator Activated Receptor alpha	Ppara	mmPPARa	TCATACATGACATGGAGAC-CTTG	ACTGGCAGCAGTGGAA-GAATC	113
Uncoupling protein 1	Ucp1	mmUCP1	CGACTCAGTCCAAGAG-TACTTCTCTTC	GCCGGCTGA-GATCTTGTTTC	72
Uncoupling protein 3	Ucp3	mmUCP3b	GAGATGGTGACCTACGA-CATCA	GCGTTCATG-TATCGGGTCTTTA	153
Fatty acid synthase	Fasn	mmFASN	GGAGGTGGTGATAGCCGGTAT	TGGGTAATCCATAGAGC-CCAG	139
Carnitine palmitoyltransferase 1C	Cpt1c	mmCPT1c-2	GAGCCATGGACAACAAG-GAGA	CAGCCATTGCTGCGACTG	197
Glucokinase	Gck	mmGck	CACATGTGCTCAGCAGGACT	AGCTTGTACACGGAGC-CATC	107
Hexokinase 1	Hk1	mmHk1	GAGGCATCTTCGAGACCAAG	TCTCGGATCTTTTCCAC-CAC	205

between males and females. Cochleae were fixed in 2% paraformaldehyde/3% glutaraldehyde in phosphate-buffered saline (PBS) overnight, then decalcified in 0.1 M EDTA in PBS for 5 days at 4°C, using established methods (32). Groups included four mutant (8 cochleae) and three control (6 cochleae) mice at ∼3 months of age. Glycol methacrylate plastic sections of 6 μm thickness were stained with hematoxylin.

Locotronic® test

To evaluate the effect of the *Tbl1xr1* mutation on locomotor coordination and the balance of mice, the Locotronic® Locomotor Test (Intellibio, France) was used (33). Mice at the age of 10 weeks traverse a horizontal ladder with evenly spaced rungs, along a narrow corridor to reach the exit. The number of errors (when the mouse foot/tail slipped between rungs) was recorded automatically. Each animal was tested three times. The more errors, the worse the psychomotor development of mice (33,34).

T3, T4 and TSH plasma concentrations

Male and female mice at the age of 12 weeks were killed by exsanguination and trunk blood was taken at the same time. Plasma was separated by centrifugation and immediately frozen at −80°C. Serum T3 and T4 were measured with in-house radioimmunoassay (35). TSH levels were measured by a mouse pituitary magnetic bead panel for TSH (the Milliplex assay), following the manufacturer's instructions (Merck-Millipore Corp., Darmstadt, Germany), and read on a BioPlex (BioRad). The obtained values were expressed in picograms per milliliter (pg/ml). All samples from one experiment were measured within the same assay.

Fluorescence *in situ* hybridization

Brains were removed, immediately frozen in 2-methylbut ane on dry ice and stored at −80°C until further processing. Coronal cryo-sections (20 μm) containing the paraventricular nucleus (PVN) were pre-treated as described before (36). In brief, defrosted and air-dried sections were fixed for 1 h in 4% PFA in PBS (pH 7.4), permeabilized in PBS containing 0.4% Triton X-100, and acetylated in 0.1 M tri-ethanolamine (pH 8.0) containing 0.25% (v/v) acetic anhydride. Subsequently, sections were dehydrated in rising concentrations of ethanol and air-dried. Third-generation fluorescence *in situ* hybridization (FISH) experiments were carried out as described previously (37,38). A probe against TRH consisting of a set of 20 individual sequences for the target was commercially designed and generated (Molecular Instruments). All buffers and amplifiers were obtained from Molecular Instruments. Sections were incubated for 10 min with hybridization buffer at 37°C before probe in hybridization buffer (0.4 pmol per 100 μl) was applied. Hybridization was carried out at 37°C for 20 h. Following rinsing with probe wash buffer and 5× SSC + 0.1% Tween20 (SSCT), sections were incubated with amplification buffer for 30 min.

Table 2. List of significant gene sets related to adipogenesis

Name [a]	Gene set	Description	N[b]	Direction	Effect	P-value[c]	FDR[d]
M2432	VERNOCHET_ADIPOGENESIS	Genes upregulated during adipogenic differentiation of 3T3-L1 cells and downregulated by troglitazone	17	↓	Less adipogenesis	0.00	0.00004
M2271	STEGER_ADIPOGENESIS_DN	Genes downregulated during adipogenesis of 3T3-L1 cells	25	↓	More adipogenesis	0.00	0.00028
M2182	WANG_CLASSIC_ADIPOGENIC_TARGETS_OF_PPARG	Classic adipogenic genes that are induced by PPARγ during adipogenesis in 3T3-L1 preadipocytes.	25	↓	Less adipogenesis	0.00	0.00063
M2270	STEGER_ADIPOGENESIS_UP	Genes upregulated during adipogenesis of 3T3-L1 cells.	21	↓	Less adipogenesis	0.00	0.00141
M1579	BURTON_ADIPOGENESIS_8	Progressively downregulated during differentiation of 3T3-L1 cells into adipocytes.	77	↓	More adipogenesis	0.00	0.00154
M1645	LI_ADIPOGENESIS_BY_ACTIVATED_PPARG	Adipocyte genes induced in 3T3-L1 cells by constitutively active PPARγ or its agonist TZD.	17	↓	Less adipogenesis1	0.00	0.00263
M1577	BURTON_ADIPOGENESIS_3	Strongly upregulated during differentiation of 3T3-L1 cells into adipocytes.	99	↑	More adipogenesis	0.00	0.00807
M1626	BURTON_ADIPOGENESIS_PEAK_AT_0HR	Downregulated during differentiation of 3T3-L1 into adipocytes in response to adipogenic hormones.	60	↓	More adipogenesis	0.00	0.00945
M2420	WAKABAYASHI_ADIPOGENESIS_PPARG_RXRA_BOUND_WITH_H4K20ME1_MARK	Genes upregulated during adipocyte differentiation of 3T3-L1 cells and newly modified by H4K20me1.	146	↓	Less adipogenesis	0.00	0.02537
M1675	GERHOLD_ADIPOGENESIS_UP	Selected genes upregulated during differentiation of 3T3-L1 cells into adipocytes in response to adipogenic hormones	47	↓	Less adipogenesis	0.00	0.02838

[a]Systematic name in MSigDB. [B]Number of genes in set. [c]Two-tailed *P*-value. [d]Benjamini and Hochberg FDR adjusted *P*-value.

Probe initiator-specific hairpins h1 and h2 labeled with AxF647 (6 pmol per 100 μl amplification buffer) were separately heat-shocked for 90 s at 95°C and cooled down at room temperature for 30 min. Hairpins were mixed in amplification buffer and applied onto the sections. Signal amplification was performed for 20 h, sections were rinsed in SSCT, incubated for 5 min with Hoechst33258 (1:2000) and cover-slipped using Fluoromount (Sigma-Aldrich). Pictures were taken on a confocal microscope (Leica SP8) as z-stacks. For TRH quantification, those optical sections from the z-stacks with the most intense TRH signals were used. TRH signal integrated density in the PVN was measured in ImageJ and background determined in a signal-free area was subtracted. Four to eight sections from 5 to 6 animals per group were analyzed.

RNA isolation and qPCR

Total RNA from liver, WAT, BAT and gastrocnemius muscle was isolated using TriReagent (Sigma) and the ISOLATE II RNA Mini Kit (BIOLINE). RNA yield was determined using the Nanodrop (Nanodrop) and cDNA was synthesized with equal RNA input with the First-Strand cDNA synthesis kit (AMV) for qPCR with oligo-d (T) primers (Roche Molecular Biochemicals). As a control for genomic DNA contamination, a cDNA synthesis reaction without reverse transcriptase was included. Quantitative PCR was performed using the LightCycler 480 (Roche Molecular Biochemicals) and LightCycler 480 SYBR Green I Master mix (Roche Molecular Biochemicals). The primers used for qPCR are listed in Table 1. Quantification was performed using the LinReg software. PCR efficiency was checked individually and samples with a deviation of more than 5% of the mean were excluded from the analysis. Calculated values were related to the geometric mean expression of the reference genes *Eef1a1*, *Rplp0* and *Hprt*, all showing stable expression under the experimental conditions.

RNA library preparation

Total RNA was extracted from WAT of 12 mice (six *Tbl1xr1*$^{Y446C/Y446C}$ mice and six WT mice; three males and three females of each genotype). To create cDNA libraries, samples were prepared using the Kapa mRNA Hyperprep kit (Roche, Basel, Switzerland). Concentration of the library samples was measured using the

Quant-it DNA HS assay (Thermo Fisher Scientific, Waltham, MA, USA). Libraries were equimolar pooled and the pool was checked on Tapestation using DNA1000 ScreenTape (Agilent Technologies, Santa Clara, CA, USA). The libraries were sequenced on the NovaSeq6000 PE150 sequencer (Illumina, San Diego, CA, USA), producing at least 40 M 150-bp paired-end reads per library.

RNA sequencing of WAT and data analysis

RNA sequencing data analyses were carried out with Bioconductor (v3.13) packages in R (v4.1.0). Raw sequencing data were subjected to quality control using FastQC (v0.11.15) and dupRadar (v1.0.0) (39,40). All samples were of sufficient quality and kept for analysis. Reads were trimmed for adapter sequences with Trimmomatic (v0.36) (41). Trimmed reads were aligned to the *Mus musculus* genome (Ensembl GRCm38v93) using HISAT2 (v2.1.0) (42). Gene level counts were obtained using HTSeq (v0.11) (43) with default parameters except -stranded = reverse and the mouse GTF from Ensembl (release 93). Additional gene annotation was retrieved from Ensembl (release 104) using the biomaRt R/Bioconductor (v2.48.1) (44). Genes with more than 2 count-per-million reads (CPM) in three or more of the samples were kept. Counts were normalized using the trimmed mean of M values normalization method of edgeR (3.34.0) (45). Then, count data were transformed to log2-counts per million (logCPM) using voom, estimating the mean–variance relationship (46). Differential expression was assessed with an empirical Bayes moderated t-test using the linear model framework from the limma package including the precision weight estimated by voom and adjusting for gender (47). The Benjamini–Hochberg FDR method was used to correct for multiple testing of resulting *P*-values.

GSEA was performed using CAMERA (limma package) with a preset value of 0.01 for the intergene correlation (48) using the Hallmark, C1, C2, C3, C5, C6, C7 and C8 gene set collections retrieved from the Molecular Signatures Database (v7.4; Entrez Gene ID version) (49). Entrez gene IDs were mapped from mouse to human with HomoloGene (v68). *P*-values were calculated for each gene set for two alternative hypotheses ('up' or 'down') and adjusted using the Benjamini–Hochberg FDR. Gene sets with an FDR adjusted *P*-value of <0.05 were considered significant. The RNA sequencing data have been deposited in NCBI Gene Expression Omnibus (GEO) and are accessible under GEO Series accession number GSE198787.

Statistical analysis

Data are expressed as mean ± standard error of the mean (SEM). Variations between *Tbl1xr1*$^{Y446C/Y446C}$ and WT mice were evaluated by two-way ANOVA using Graphpad Prism 9.0 software with two grouping factors (gender and strain) followed by Tukey *post hoc* analysis. If there was no difference between genders, data of male and female mice were pooled. Statistical significance was defined at a level of $P < 0.05$.

Supplementary Material

Supplementary Material is available at *HMGJ* online.

Acknowledgements

We would like to thank Olga Surovtseva (Endocrine Laboratory) for expert help with RNA isolation and qPCR as well as the staff of the Endocrine Laboratory for measuring serum thyroid hormones and TSH.

Conflict of Interest statement. The authors report no conflict of interest.

Funding

Chinese Scholarship Council (CSC) (201907720056 to Y.H.); National Institutes of Health (to L.N. and D.F.).

References

1. Pierpont, M.E., Stewart, F.J. and Gorlin, R.J. (1998) Plantar lipomatosis, unusual facial phenotype and developmental delay: a new MCA/MR syndrome. *Am. J. Med. Genet.*, **75**, 18–21.
2. Oudesluijs, G.G., Hordijk, R., Boon, M., Sijens, P.E. and Hennekam, R.C. (2005) Plantar lipomatosis, unusual facies, and developmental delay: confirmation of Pierpont syndrome. *Am. J. Med. Genet. A*, **137**, 77–80.
3. Vadivelu, S., Edelman, M., Schneider, S.J. and Mittler, M.A. (2013) Choroid plexus papilloma and Pierpont syndrome. *J. Neurosurg. Pediatr.*, **11**, 115–118.
4. Heinen, C.A., Jongejan, A., Watson, P.J., Redeker, B., Boelen, A., Boudzovitch-Surovtseva, O., Forzano, F., Hordijk, R., Kelley, R., Olney, A.H. *et al.* (2016) A specific mutation in TBL1XR1 causes Pierpont syndrome. *J. Med. Genet.*, **53**, 330–337.
5. Jain, B.P. and Pandey, S. (2018) WD40 repeat proteins: signalling scaffold with diverse functions. *Protein J.*, **37**, 391–406.
6. Stirnimann, C.U., Petsalaki, E., Russell, R.B. and Muller, C.W. (2010) WD40 proteins propel cellular networks. *Trends Biochem. Sci.*, **35**, 565–574.
7. Ng, L., Kelley, M.W. and Forrest, D. (2013) Making sense with thyroid hormone—the role of T3 in auditory development. *Nat. Rev. Endocrinol.*, **9**, 296–307.
8. Heinen, C.A., Losekoot, M., Sun, Y., Watson, P.J., Fairall, L., Joustra, S.D., Zwaveling-Soonawala, N., Oostdijk, W., van den Akker, E.L., Alders, M. *et al.* (2016) Mutations in TBL1X are associated with central hypothyroidism. *J. Clin. Endocrinol. Metab.*, **101**, 4564–4573.
9. Di Stazio, M., Collesi, C., Vozzi, D., Liu, W., Myers, M., Morgan, A., P, A., D, A., Girotto, G., Rubinato, E., Giacca, M. *et al.* (2019) TBL1Y: a new gene involved in syndromic hearing loss. *Eur. J. Hum. Genet.*, **27**, 466–474.
10. Lu, J., Bang, H., Kim, S.M., Cho, S.J., Ashktorab, H., Smoot, D.T., Zheng, C.H., Ryeom, S.W., Yoon, S.S., Yoon, C. *et al.* (2021) Lymphatic metastasis-related TBL1XR1 enhances stemness and metastasis in gastric cancer stem-like cells by activating ERK1/2-SOX2 signaling. *Oncogene*, **40**, 922–936.
11. Zhou, Q., Xu, M., Wang, X., Yu, M., Chen, X., Lu, J., Zhou, R., Zhang, J., Ling, X. and Ji, J. (2021) Deficiency of TBL1XR1 causes asthenozoospermia. *Andrologia*, **53**, e13980.
12. Ismaili-Jaha, V., Spahiu-Konusha, S. and Jaha, A. (2021) Pierpont syndrome-report of a new patient. *Clin. Case Rep.*, **9**, 2113–2116.

13. Yan, H.T., Shinka, T., Kinoshita, K., Sato, Y., Umeno, M., Chen, G., Tsuji, K., Unemi, Y., Yang, X.J. and Iwamoto, T. (2005) Molecular analysis of TBL1Y, a Y-linked homologue of TBL1X related with X-linked late-onset sensorineural deafness. *J. Hum. Genet.*, **50**, 175–181.
14. Berger, J.P., Akiyama, T.E. and Meinke, P.T. (2005) PPARs: therapeutic targets for metabolic disease. *Trends Pharmacol. Sci.*, **26**, 244–251.
15. Klingenberg, M. and Lin, C.S. (1986) Isolation and hydrodynamic characterization of the uncoupling protein from brown adipose tissue. *Methods Enzymol.*, **126**, 490–498.
16. Lin, C.S. and Klingenberg, M. (1980) Isolation of the uncoupling protein from brown adipose tissue mitochondria. *FEBS Lett.*, **113**, 299–303.
17. Cannon, B. and Nedergaard, J. (2004) Brown adipose tissue: function and physiological significance. *Physiol. Rev.*, **84**, 277–359.
18. Villarroya, F., Iglesias, R. and Giralt, M. (2007) PPARs in the control of uncoupling proteins gene expression. *PPAR Res.*, **2007**, 74364.
19. Hondares, E., Rosell, M., Díaz-Delfín, J., Olmos, Y., Monsalve, M., Iglesias, R., Villarroya, F. and Giralt, M. (2011) Peroxisome proliferator-activated receptor α (PPARα) induces PPARγ coactivator 1α (PGC-1α) gene expression and contributes to thermogenic activation of brown fat. *J. Biol. Chem.*, **286**, 43112–43122.
20. Barbera, M.J., Schluter, A., Pedraza, N., Iglesias, R., Villarroya, F. and Giralt, M. (2001) Peroxisome proliferator-activated receptor alpha activates transcription of the brown fat uncoupling protein-1 gene. A link between regulation of the thermogenic and lipid oxidation pathways in the brown fat cell. *J. Biol. Chem.*, **276**, 1486–1493.
21. Gordon, D.M., Neifer, K.L., Hamoud, A.A., Hawk, C.F., Nestor-Kalinoski, A.L., Miruzzi, S.A., Morran, M.P., Adeosun, S.O., Sarver, J.G., Erhardt, P.W. *et al.* (2020) Bilirubin remodels murine white adipose tissue by reshaping mitochondrial activity and the coregulator profile of peroxisome proliferator-activated receptor alpha. *J. Biol. Chem.*, **295**, 9804–9822.
22. Lidell, M.E., Betz, M.J., Dahlqvist Leinhard, O., Heglind, M., Elander, L., Slawik, M., Mussack, T., Nilsson, D., Romu, T., Nuutila, P. *et al.* (2013) Evidence for two types of brown adipose tissue in humans. *Nat. Med.*, **19**, 631–634.
23. Lee, P., Werner, C.D., Kebebew, E. and Celi, F.S. (2014) Functional thermogenic beige adipogenesis is inducible in human neck fat. *Int. J. Obes.*, **38**, 170–176.
24. Song, Z., Xiaoli, A.M. and Yang, F. (2018) Regulation and metabolic significance of *de novo* lipogenesis in adipose tissues. *Nutrients*, **10**, 1383.
25. Ogino, S., Kawasaki, T., Ogawa, A., Kirkner, G.J., Loda, M. and Fuchs, C.S. (2007) Fatty acid synthase overexpression in colorectal cancer is associated with microsatellite instability, independent of CpG island methylator phenotype. *Hum. Pathol.*, **38**, 842–849.
26. Berndt, J., Kovacs, P., Ruschke, K., Kloting, N., Fasshauer, M., Schon, M.R., Korner, A., Stumvoll, M. and Bluher, M. (2007) Fatty acid synthase gene expression in human adipose tissue: association with obesity and type 2 diabetes. *Diabetologia*, **50**, 1472–1480.
27. Okamura, M., Inagaki, T., Tanaka, T. and Sakai, J. (2010) Role of histone methylation and demethylation in adipogenesis and obesity. *Organ*, **6**, 24–32.
28. Gulyaeva, O., Dempersmier, J. and Sul, H.S. (2019) Genetic and epigenetic control of adipose development. *Biochim. Biophys. Acta Mol. Cell Biol. Lipids*, **1864**, 3–12.
29. Mottillo, E.P., Balasubramanian, P., Lee, Y.H., Weng, C., Kershaw, E.E. and Granneman, J.G. (2014) Coupling of lipolysis and *de novo* lipogenesis in brown, beige, and white adipose tissues during chronic beta3-adrenergic receptor activation. *J. Lipid Res.*, **55**, 2276–2286.
30. Mianne, J., Codner, G.F., Caulder, A., Fell, R., Hutchison, M., King, R., Stewart, M.E., Wells, S. and Teboul, L. (2017) Analysing the outcome of CRISPR-aided genome editing in embryos: screening, genotyping and quality control. *Methods*, **121–122**, 68–76.
31. Rusch, A., Ng, L., Goodyear, R., Oliver, D., Lisoukov, I., Vennstrom, B., Richardson, G., Kelley, M.W. and Forrest, D. (2001) Retardation of cochlear maturation and impaired hair cell function caused by deletion of all known thyroid hormone receptors. *J. Neurosci.*, **21**, 9792–9800.
32. Ng, L., Cordas, E., Wu, X., Vella, K.R., Hollenberg, A.N. and Forrest, D. (2015) Age-related hearing loss and degeneration of cochlear hair cells in mice lacking thyroid hormone receptor beta1. *Endocrinology*, **156**, 3853–3865.
33. Rousselet, E., Joubert, C., Callebert, J., Parain, K., Tremblay, L., Orieux, G., Launay, J.-M., Cohen-Salmon, C. and Hirsch, E.C. (2003) Behavioral changes are not directly related to striatal monoamine levels, number of nigral neurons, or dose of parkinsonian toxin MPTP in mice. *Neurobiol. Dis.*, **14**, 218–228.
34. Chort, A., Alves, S., Marinello, M., Dufresnois, B., Dornbierer, J.G., Tesson, C., Latouche, M., Baker, D.P., Barkats, M., El Hachimi, K.H. *et al.* (2013) Interferon beta induces clearance of mutant ataxin 7 and improves locomotion in SCA7 knock-in mice. *Brain*, **136**, 1732–1745.
35. Wiersinga, W.M. and Chopra, I.J. (1982) Radioimmunoassay of thyroxine (T4), 3,5,3′-triiodothyronine (T3), 3,3′,5′-triiodothyronine (reverse T3, rT3), and 3,3′-diiodothyronine (T2). *Methods Enzymol.*, **84**, 272–303.
36. Heuer, H., Schafer, M.K., O'Donnell, D., Walker, P. and Bauer, K. (2000) Expression of thyrotropin-releasing hormone receptor 2 (TRH-R2) in the central nervous system of rats. *J. Comp. Neurol.*, **428**, 319–336.
37. Choi, H.M.T., Schwarzkopf, M., Fornace, M.E., Acharya, A., Artavanis, G., Stegmaier, J., Cunha, A. and Pierce, N.A. (2018) Third-generation *in situ* hybridization chain reaction: multiplexed, quantitative, sensitive, versatile, robust. *Development*, **145**, dev165753.
38. Mayerl, S., Chen, J., Salveridou, E., Boelen, A., Darras, V.M. and Heuer, H. (2022) Thyroid hormone transporter deficiency in mice impacts multiple stages of GABAergic interneuron development. *Cereb. Cortex*, **32**, 329–341.
39. Sayols, S., Scherzinger, D. and Klein, H. (2016) dupRadar: a bioconductor package for the assessment of PCR artifacts in RNA-Seq data. *BMC Bioinform.*, **17**, 428.
40. Andrews, S. (2010) FastQC. A quality control tool for high throughput sequence data. https://www.bioinformatics.babraham.ac.uk/projects/fastqc/.
41. Bolger, A.M., Lohse, M. and Usadel, B. (2014) Trimmomatic: a flexible trimmer for Illumina sequence data. *Bioinformatics*, **30**, 2114–2120.
42. Kim, D., Paggi, J.M., Park, C., Bennett, C. and Salzberg, S.L. (2019) Graph-based genome alignment and genotyping with HISAT2 and HISAT-genotype. *Nat. Biotechnol.*, **37**, 907–915.
43. Anders, S., Pyl, P.T. and Huber, W. (2015) HTSeq—a Python framework to work with high-throughput sequencing data. *Bioinformatics*, **31**, 166–169.
44. Howe, K.L., Achuthan, P., Allen, J., Allen, J., Alvarez-Jarreta, J., Amode, M.R., Armean, I.M., Azov, A.G., Bennett, R.,

Bhai, *J. et al.* (2021) Ensembl 2021. *Nucleic Acids Res.*, **49**, D884–d891.

45. Robinson, M.D. and Oshlack, A. (2010) A scaling normalization method for differential expression analysis of RNA-seq data. *Genome Biol.*, **11**, R25.
46. Law, C.W., Chen, Y., Shi, W. and Smyth, G.K. (2014) voom: precision weights unlock linear model analysis tools for RNA-seq read counts. *Genome Biol.*, **15**, R29.
47. Ritchie, M.E., Phipson, B., Wu, D., Hu, Y., Law, C.W., Shi, W. and Smyth, G.K. (2015) Limma powers differential expression analyses for RNA-sequencing and microarray studies. *Nucleic Acids Res.*, **43**, e47.
48. Wu, D. and Smyth, G.K. (2012) Camera: a competitive gene set test accounting for inter-gene correlation. *Nucleic Acids Res.*, **40**, e133.
49. Subramanian, A., Tamayo, P., Mootha, V.K., Mukherjee, S., Ebert, B.L., Gillette, M.A., Paulovich, A., Pomeroy, S.L., Golub, T.R., Lander, E.S. *et al.* (2005) Gene set enrichment analysis: a knowledge-based approach for interpreting genome-wide expression profiles. *Proc. Natl. Acad. Sci. U.S.A.*, **102**, 15545–15550.